RSC Advances

ROYAL SOCIETY OF CHEMISTRY

www.rsc.org/advances

RSC Advances

ARTICLE

Time-Resolved SANS Analysis of Micelle Chain Exchange Behavior: Thermal Crosslink Driven by Stereocomplexation of PLA-PEG-PLA Micelles

Received 00th January 20xx,
Accepted 00th January 20xx

DOI: 10.1039/x0xx00000x

www.rsc.org/

Daniel G. Abebe[a], Kwei-Yu Liu[a], Sanjay Mishra[b], Alex Wu[c], Robert Lamb[c], Tomoko Fujiwara*[a]

Time-resolved small-angle neutron scattering (TR-SANS) was used to study the dynamic chain exchange behavior of the micelle mixture from poly(L-lactide)-*b*-poly(ethylene glycol)-*b*-poly(L-lactide), PLLA-PEG-PLLA, and its enantiomeric copolymer, PDLA-PEG-PDLA. The mixture of enantiomeric micelle solutions underwent sol-to-gel transition as a consequence of temperature increase to yield a thermo-responsive hydrogel. The mechanism of gelation is hypothesized as a chain exchange process between L-micelles and D-micelles followed by the formation of stereocomplex crystals from PLLA and PDLA blocks. Stereocomplex crystals that have different physicochemical properties from PLLA or PDLA crystals restrain further chain exchange ability, which results in a network structure. We investigated the changes in micelle re-organization given by the SANS intensity as a function of q-range, over time ranging from one to twenty minutes. TR-SANS data supported the hypothesis, that single and stereo-mixed micelle systems undergo equilibrium and non-equilibrium chain exchange behaviors, respectively. We observed considerable difference in the scattering profile for the stereo-mixed micelles due to the structural re-organization from original micelle to bridged micelle network. The molecular weight of the hydrophilic PEG block was shown to influence the intermicellar interaction and chain exchange rate; short PEG micelles exhibited faster chain exchange behavior which was correlated to the lower sol-to-gel transition temperature observed.

Introduction

Block copolymer micelles self-assembled in a selective solvent have been utilized for various purposes, such as drug delivery carriers and imaging agents.[1] Two important factors that influence their applicability are the micelle stability and their dynamic behavior in solution. Specifically, the chain exchange between the micelles in solution is a subject of investigation for many copolymer systems. While several techniques have been used to study micelle dynamics,[2-5] small angle neutron scattering (SANS) has been employed with considerable success in elucidating the chain exchange behavior of polymeric micelles. Lund et al. studied the equilibrium chain exchange kinetics of several di- and triblock copolymers using SANS by mixing hydrogenated (h) and deuterated (d) micelles under zero average contrast conditions.[6-8] Exchange of polymer chains between the (h)/(d) micelles then leads to a decrease in contrast and decay of the scattered neutron intensity. Using time-resolved SANS (TR-SANS), they obtained relaxation time constants for the chain exchange processes. They concluded that the exchange occurred through an expulsion/insertion mechanism involving only single chain at a given time, of which the chain expulsion is the rate-determining step.

Micelles prepared from the block copolymers of biodegradable poly(lactic acid) (PLA) and poly(ethylene glycol) (PEG) have been widely studied as drug delivery carriers. Several groups have reported SANS studies for PLA-PEG micelles. Riley and Davis investigated the nanostructure and chain conformation using SANS.[9] Contrast match studies using selectively deuterated PLA(d)-PEG diblock copolymers confirmed the formation of spherical core-shell particles, where the hydrophobic PLA blocks aggregate to form a homogeneous core of uniform scattering length density and the hydrophilic PEG block forms the stabilizing shell (corona) of the particle. Both particle size and conformation of the PEG chains varied depending on the PLA block length. Tew et al., in contrast, used all hydrogenated triblock copolymers, PLA-PEG-PLA, to study the infinity structure of their micelles in deuterium oxide (D_2O) using SANS.[10] They investigated the effects of stereo-regularity and block length of PLA on particle morphology and size. The triblock copolymers with stereo-regular PLLA block (semi-crystal) and racemic PDLLA block (amorphous) in aqueous medium at relatively high concentration led to non-spherical lamellar core micelle and spherical micelle, respectively. The variation in the block

[a] Department of Chemistry, The University of Memphis, Memphis, TN 38152, USA.
[b] Department of Physics, The University of Memphis, Memphis, TN 38152, USA.
[c] School of Chemistry, The University of Melbourne, Parkville Vic. 3010, Australia.
† To whom correspondence should be addressed. Phone: +1-901-678-5558, E-mail: tfjiwara@memphis.edu.
Electronic Supplementary Information (ESI) available: [Complete model fitting results and representative fits of the scattering spectra]. See
DOI: 10.1039/x0xx00000x

lengths of PLLA and PDLLA affected the micelle dimensions, such as the core radius, aggregation number, and crystallite thickness. The effect of polymer concentration was also examined; at higher concentrations macro-aggregation was observed due to chain exchange between nearby micelles resulting in network and gel formation.

Hydrogels derived from PLA-PEG micelles are promising biomaterials as drug delivery carriers and temporary implants.[11-16] Fujiwara and Kimura applied new gelation mechanism of stereocomplex crystal formation using copolymers of enantiomeric PLAs, PLLA-PEG-PLLA and PDLA-PEG-PDLA, and found a thermo-responsive sol-to-gel transition behavior.[17, 18] Recently, we developed stereocomplex hydrogels with high mechanical properties and temperature controllable sol-to-gel transitions.[19] The sol-to-gel transition mechanism of stereo-mixture (1:1 mixture of PLLA-PEG-PLLA micelles and PDLA-PEG-PDLA micelles) is hypothesized as the result of stereocomplex crystal formation by PLLA and PDLA blocks after chain exchange occurred between those micelles. Physicochemical properties of PLLA/PDLA stereocomplex crystals are considerably different from PLLA or PDLA homo-crystals; for example, the stereocomplex crystals possess a tighter packing crystal lattice, higher melting point, and lower solubility in most of solvents compared to homo-crystals. Therefore, chain mobility of the micelles after stereocomplex formation should be restrained (i.e. crosslinked), which would be a driving force for transition into a hydrogel network structure. In a recent study by He and co-workers, stereocomplexation between enantiomeric PLA's was utilized to greatly enhance the stability of pH responsive micelles composed of PDMAEMA-b-PDLA-b-PDMAEMA-g-PEG and PDMAEMA-b-PLLA-b-PDMAEMA-g-PEG copolymers by physically crosslinking the core.[20] The use of stereocomplexation as a crosslinking method is highly desirable for the preparation of next generation biomaterials due to the increased biocompatibility and readily applicable technique.

In this study, we used TR-SANS to study the dynamic chain exchange behavior of enantiomeric micelle mixture of all hydrogenated PLLA-PEG-PLLA and PDLA-PEG-PDLA in D_2O during the initial stages of the sol-to-gel transition process. Moreover, we compared the mobility of the PLA blocks in the core by varying the length of PEG (MW = 2000 and 3350) in the triblock copolymer. Model dependent analysis of the SANS data was performed and calculated parameters are presented. Table 1 lists the triblock copolymers and 'ID' of their micelles used in this report. It has to be noted here; although we have confirmed a hydrogel formation for the mixture of 10 wt% **L-short** and **D-short** micelles or **L-long** and **D-long** micelles upon heating, the SANS study we report here is focused on initial dynamics in water where all systems are still in solution state.

Experimental Section

Table 1. Triblock copolymers used for the SANS study

Copolymer	MW (Da)	Micelle ID
$PLLA_{11}$-PEG_{45}-$PLLA_{11}$	800-2000-800	L-short
$PDLA_{11}$-PEG_{45}-$PDLA_{11}$	800-2000-800	D-short
$PLLA_{11}$-PEG_{76}-$PLLA_{11}$	800-3350-800	L-long
$PDLA_{11}$-PEG_{76}-$PDLA_{11}$	800-3350-800	D-long

Synthesis of PLA-PEG-PLA triblock copolymers

The ABA-type triblock copolymers, PLLA-PEG-PLLA and PDLA-PEG-PDLA were prepared by ring-opening polymerization (ROP) of L-lactide and D-lactide respectively, with PEG-2000 or PEG-3350 as the macroinitator. Detailed synthesis description can be found in our previous report.[19] The chemical structure, composition, molecular weight and polydispersity were determined using ^{1}HNMR and GPC techniques. These results are provided in the supporting information (Table S1 and Figure S1).

Micelle formation

The micelle solutions of the PLA-PEG-PLA triblock copolymers were prepared using the nanoprecipitation method. Briefly, the PLLA-PEG-PLLA or the PDLA-PEG-PDLA copolymer was dissolved in tetrahydrofuran (THF). The transparent organic solution was added dropwise into D_2O with an ultrasonic wave applied at ~4°C. The organic solvent (THF) was then evaporated from the suspension in a fume hood under a gentle stream of air to acquire an aqueous micelle solution. Micelle concentrations of 1, 5 and 10 wt% were prepared for various analyses. For SANS data, only the results from 5 wt% micelle solutions are discussed in this paper.

SANS Experiment

The SANS experiment was conducted on the NG-7 30m beamline at the National Institute for Standard and Technology (NIST), Gaithersburg, MD. Scattering range used in this time-resolved study was 0.1<q<0.01 Å-1 which correspond to a detector distance of 4.0 m. All measurements were run on quartz sample cells with path length of 2 mm and an incident wavelength of 6.0 Å with a wavelength spread ($(\Delta\lambda/\lambda)$ of 0.12 was used. All measurements were done in 100 % D_2O medium at 25°C, 37°C and 45°C. For kinetic measurement studies, scattering was collected every minute for 20 minutes for blend solution (PLLA + PDLA) and 10 minutes for non-blend solutions (PLLA). For non-kinetic measurements, spectra were collected between 10 to 30 minutes. The following equation was used to calculate the scattering length density (SLD)(ρ) of the monomers,[21]

$$\rho = \frac{\rho_m N_A}{\mathrm{M}} \sum_i n_i b_i \qquad (1)$$

where ρ_m is the bulk density of the polymer, N_A is Avogadro's number, M is monomer molecular weight, n_i is the number of atoms in the monomer and b_i is the scattering length of each atom in the monomer. The computed SLD values for each monomer are given in Table S2. The scattering and transmission of each

sample was measured at each temperature, scattering data was corrected for transmission and background. The scattering data were reduced and modeled using data reduction and modeling software provided by NIST[22] and reported on an absolute scale except where noted

Results and Discussion

Gelation mechanism of stereo-enantiomeric micelles

Amphiphilic block copolymers, PLA-PEG-PLA, self-assemble into micelles when placed in an aqueous environment. The hydrophobic PLA outer blocks aggregate in the core stabilized by a corona of the hydrophilic PEG middle blocks. At some particular temperature, the mobility of the PLA core blocks increases, with enough energy for expulsion from the core and insertion to a neighbouring micelle. With increasing temperature or time, the rate of the PLA block exchange between micelles is increased. The PEG block acts as a bridge (physical cross-linker) between the micelles to establish a network. Figure 1 illustrates the plausible mechanisms of those micelles in relatively dilute aqueous solution (5-10 wt%). For the L-isomeric micelles (PLLA), the chain exchange is not immediately the driving force of network formation as PLLA blocks in every micelle core still keep their mobility (Figure 1a). Therefore, gel formation does not occur, or is negligible. In the same condition, if 50 % of micelles are from D-isomeric copolymer, the chain exchange between L-micelles and D-micelles causes stereocomplex crystal formation in the core, which irreversibly changes the core properties (Figure 1b). We used WAXS analysis to confirm the formation of stereocomplex crystals during sol-to-gel transformation with increasing temperature. The WAXS profiles of the freeze-dried micelles used in this study is provided in Supplementary Information (Figure S2). The diffraction curve (Figure S2a I-IV) for the stereo-mixed micelles of **L-short/D-short** system showed PLLA homo-crystal peaks at 2θ = 17° and 19°, crystalline PEG at 2θ = 19° (overlapped with PLLA peak) and 23°, and the stereocomplex diffraction pattern at 2θ = 12° and 21°. The intensity of the stereocomplex diffraction peaks continued to increase upon heating while that of the homo crystal peak decreased, which indicated continuous chain exchange of PLLA and PDLA blocks between micelles. The diffraction curve (Figure S2b V-VII) for the stereo-mixed micelles of **L-long/D-long** system also displayed a similar trend. The WAXS analysis shows, regardless of the PEG block length, hydrogel formation is achieved through the stereocomplexation mechanism. The repeating unit number of lactate in our copolymer systems is approximately 11. This is the lower critical size for PLA to form homo-crystals. The lower critical number for stereocomplex crystal formation at 1:1 PLLA/PDLA mixture is 7. Therefore, for the PLA-PEG-PLA copolymers reported in this study, stereocomplex formation is more favored as we have shown in our previous report by

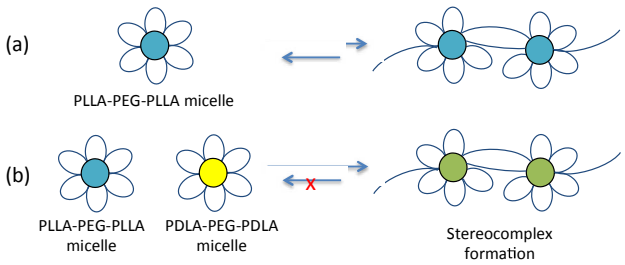

Figure 1. Proposed chain exchange mechanism of triblock copolymer micelles, a) single enantiomeric micelles, b) equimolar mixture of both enantiomeric micelles. Micelles containing either PLLA or PDLA cores are designated as blue or yellow, respectively. However, micelles containing both PLLA and PDLA within a single core are designated by the color green to emphasize the co-crystallization and formation of a new stereocomplexed crystal.

determining the enthalpy of crystal melting.[19] Also, it has been reported that the stereocomplex formation is thermodynamically favorable.[23]

Effects of PEG block size on micelle and hydrogel properties

In our previous work, we reported the modulation of the physical and mechanical properties of PLA-PEG-PLA hydrogels in response to variation in the PEG block length. We observed drastic differences in the sol-to-gel phase behavior for 10 wt% micelle solutions of **L-short/D-short** and **L-long/D-long** systems; unlike the homo-PLA micelle systems (**L-short** or **L-long**) that showed no gelation, sol-to-gel transition was observed for L/D mixed micelle systems at around 10°C (short PEG) and 70°C (long PEG).[19] This difference in sol-to-gel transition behavior is clearly seen in the WAXS profiles shown in Figure S2. The growth of the stereocomplex crystal at 2θ = 12° and 21° is relatively faster for the **L-short/D-short** (Figure S2a I-III) compared to the **L-long/D-long** (Figure S2b V-VII). Since stereocomplexation is the driving force for gel formation, chain exchange for the **L-short/D-short** system must be faster compared to **L-long/D-long** system, which can be evidenced from the sol-to-gel phase transition plot shown in Figure 2.

Further, we investigated the effect of PEG size on the hydrodynamic diameter and aggregation behavior of these PLA-PEG-PLA triblock copolymer micelles using DLS. The aqueous micelles were transparent or slightly opaque solutions without any precipitation or visible aggregation. Table S3 lists DLS result for **L-short** (PEG 2000) and **L-long** (PEG 3350) micelles. Both micelles showed bimodal peak profiles for relatively high concentration solutions, (1, 5, and 10 wt%). Figure 3 shows the superimposed DLS scattered peaks for closer analysis. Hydrodynamic diameters of peak-1 indicate individual micelle size, and those of peak-2 are detected as an aggregation peak. Relative intensity of the aggregation peak increased as polymer concentration increases. An interesting trend was seen for the aggregation peaks in which **L-short** micelle aggregates were larger in size than **L-long** aggregates in any concentration at room temperature. Furthermore, the individual micelle sizes observed in peak-1 are consistent;

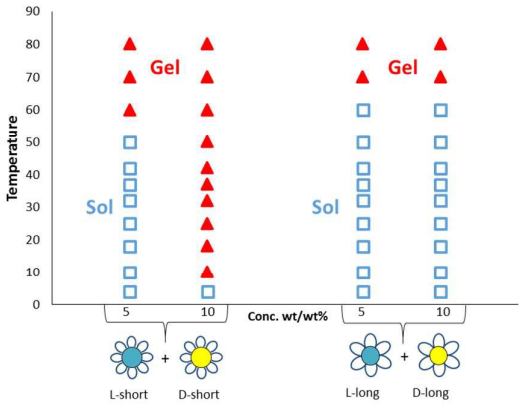

Figure 2. Comparison of the sol-to-gel transitions. (Left) Mixture of enantiomeric micelles composed of PLA-PEG(2000)-PLA (Short-PEG) show sol-to-gel transition at 60 °C and 10°C for 5 and 10 wt/wt% concentrations respectively. (Right) Mixture of enantiomeric micelles composed of PLA-PEG(3350)-PLA (Long-PEG) show sol-to-gel transition at 70 °C for both 5 and 10 wt/wt%.

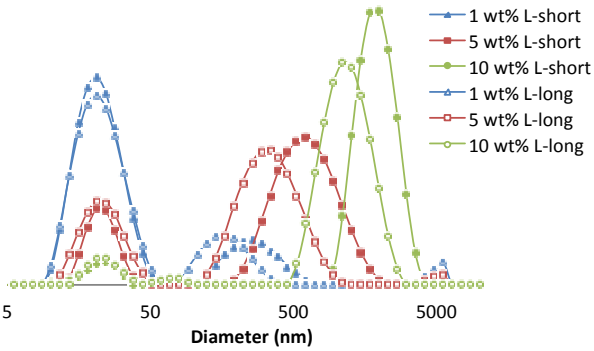

Figure 3. DLS curves of **L-short** and **L-long** micelles in 1, 5, and 10 wt% aqueous solutions at 25°C.

whereas the aggregation size drastically increases with increasing concentration. This result agrees with other reported PEGylated micelles and their aggregation behavior.[24] The tendency of the **L-short** micelles to form larger aggregates can be correlated to decreased corona repulsion and decreased micelle stability. This could explain the hypothesized fast chain exchange for the short-PEG micelles and the observed low sol-to-gel phase transition. Alternatively, the contrary would be true for the long-PEG micelles.

Chain exchange kinetic studies using TR-SANS

In this study, we set out to elucidate the chain exchange behaviour and micelle dynamics of these PLA-PEG-PLA micelle systems. Although others have reported SANS studies for these micellar systems, we focused our investigation on the effects of core-crystal forms (single vs. enantio-mixed micelles, shown in Figure 1) and corona composition (short vs. long PEG micelle, Figure 2) on the chain exchange kinetics. For our SANS study, we used 5 wt% of micelle solutions for all 4 micelle systems. As expected, 5 wt% of both **L-short** and **L-long** micelles stayed as a solution up to 70°C. The long PEG stereo-mixed micelle system, **L-long/D-long** (5 wt%) also did not show a transition to a gel form by heating up to 80°C. Only short PEG stereo-mixture, **L-short/D-short** (5 wt%) displayed sol-to-gel transition at 60°C. As shown in our previous report, gelation temperature for these systems is dependent upon concentration, by decreasing the concentration from 10 wt% to 5 wt%, we observed the sol-to-gel transition at higher temperatures, (Figure 2). It is important to emphasize that the focus of our study is on the initial chain exchange events occurring between individual micelles in solution state, as we believe such events will build up a networked macrostructure resulting into a hydrogel.

Therefore, at the temperatures (25°C and 37°C) used for SANS experiments, all four systems (**L-short**, **L-long**, **L-short/D-short**, and **L-long/D-long**) were still in solution state. Discussions of all systems henceforth only concern the initial chain exchange process of these micelles in a solution.

SANS profiles of single and enantio-mixture micelles

As illustrated in Figure 1, the PLA-PEG-PLA micelles prepared in D_2O have a spherical core-shell structure, where the PLA blocks aggregate in the core and the PEG middle blocks exist as loops on the surface, extending into solution resulting in a flower-type micelle. Figure 4 shows the typical TR-SANS curves of single isomeric copolymer micelles, **L-short**: PLLA-PEG-PLLA (800-2000-800), **L-long**: PLLA-PEG-PLLA (800-3350-800), and 1:1 mixtures of L- and D-copolymer micelles, **L-short/D-short** and **L-long/D-long** measured at 25°C and 37°C. The chart contains only time = 1 (min) and time = 10 (min) plots for each sample although data was collected every 1min in 10 or 20 min duration. All micelle solutions were prepared on site just before the SANS measurement, and kept at 4°C until the start of data collection. The L and D micelle solutions for stereo-mixed systems were then mixed at 1:1 (vol/vol) and set in the temperature-controlled sample chamber immediately before the data collection. The inset plot with expanded y-axis in Figure 4 emphasizes the differences between; (1) the single and stereo-mixed micelles and (2) short-PEG and long-PEG micelle behaviors. The former difference is seen particularly for **L-short** (blue-diamond) and **L-short/D-short** (green-square). From time = 1 (open marks) to time = 10 (closed marks), the scattering intensity of stereo-mixed micelles considerably increased relative to the small increase of single isomeric micelles at low-q range. Long-PEG series also showed the same trend (blue circle and green triangle). This result indicates a specific interaction between PLLA micelle and PDLA micelle occurred even at room temperature. The latter difference was seen as; the scattering intensity of short PEG

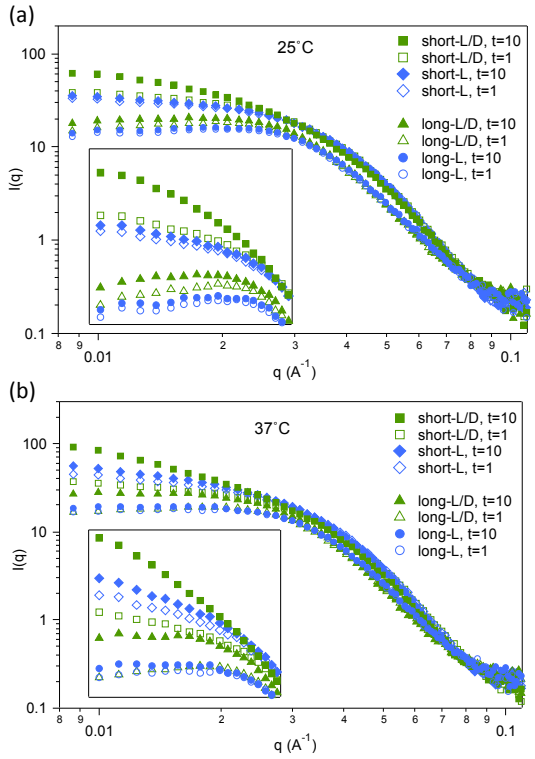

Figure 4. Scattering curves of **L-short** (blue-diamond), **L-short/D-short** (green-square), **L-long** (blue-circle), and **L-long/D-long** (green-triangle) at 25°C (a) and 37°C (b); time = 1 min (open marks) and time = 10min (closed marks). All freshly prepared single micelle solutions were kept at 4°C right before collecting data in temperature controlled sample bath.

micelles (**L-short**, **L-short/D-short**) were higher than long PEG micelles (**L-long**, **L-long/D-long**), also kept increasing at low q < 0.01 Å^{-1}. At 37°C similar trends were observed for all 4 micelle systems (Figure 4b); however, the intensity increases at t = 10 min were greater than that observed at 25°C. The short PEG micelles, particularly **L-short/D-short** system does not reach the plateau at q = 0.01 Å^{-1}. SANS measurement at lower q range (q < 0.01 Å^{-1}) would be needed for short PEG series to discuss the structural events in larger range (> 100 nm). The long PEG micelle systems displayed relatively small changes even at 37°C. Although at SANS experiment temperatures (25 and 37°C) all four systems (**L-short**, **L-long**, **L-short/D-short**, and **L-long/D-long**) were still in solution state, the SANS profiles revealed considerable difference on the degree of chain mobility and structural transformation between short PEG and long PEG stereo-mixed micelles at room temperature, and more significantly at 37 °C. Further analysis of SANS curves by model fitting will be provided later for more detailed discussion on micelle dynamics. The scattering intensity of this stereo-mixed micelle system is likely to continuously increase at the q range lower than 0.01 Å^{-1}, in which larger structural events can be expected at size range greater than 100 nm. Temperature dependent SANS experiments have been reported for several triblock copolymer micelle-hydrogel systems such as PEO-PPO-PEO[25, 26] and PLA-PEG-PLA.[10]

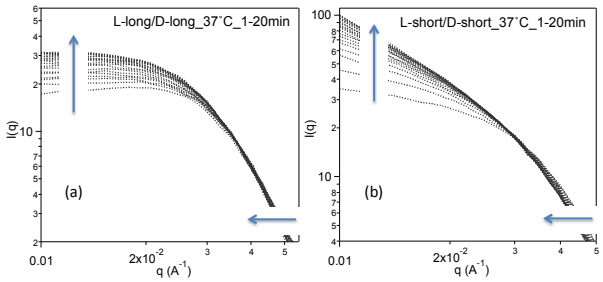

Figure 5. Shifts in Time-resolved SANS curves for initial 20min at 37°C upon mixing L/D micelles; a) **L-long/D-long** and b) **L-short/D-short** at 37°C.

For non-equilibrium chain exchange systems, the scattering intensity is related to the reorganization of micelles mediated by chain exchange between micelles. For our stereo-mixed micelle mixtures, the driving force of structural reorganization should be related to the stereocomplex crystal formation after the chain exchange event. The same trends in SANS curve shifts during the first 20 minutes were observed for all stereo-mixed micelle solutions. Figure 5 shows 20 curves for **L-long/D-long** (a) and **L-short/D-short** (b) mixtures at 37°C. In our time-resolved studies, regardless of concentration, the scattering profile of stereo-mixed micelle solutions shifted to the lower q-range as indicated by arrows in the graphs. Particularly, short PEG stereo-mixed micelles exhibited distinct peak shift to low-q at higher temperature. This result indicates that some aggregation, self-assembling process, or structural reorganization occurred between L- and D-micelles. Further analysis of structural information by fitting model was performed (vide infra).

Model independent kinetic analysis: Guinier plot analysis

The Guinier plots (ln[I(Q)] vs Q^2) were drawn in order to examine the radius of gyration (R_g). The slope of the Guinier region was modeled as a spherical scattering entity which gives the value of R_g^2/3. Figure 6 shows typical Guinier plots for **L-long/D-long** (a) and **L-short/D-short** (b). The y-axis was offset to show each plot. Fitting was applied in the q-range 0.026-0.046 Å, and the obtained R_g data had a standard deviation within 0.2 Å. All R_g data obtained were plotted against time in Figure 7. For the single **L-long** and **L-short** micelles at 25°C, R_g/R_h was calculated around 0.5 using DLS data (R_h = ca. 100 Å, from hydrodynamic diameters of 5 wt% micelles in Table S3), which is considered to be low for spherical objects (typically 0.75). However this has been observed for extensively hydrated PEGylated core-shell type micelles with high density core. [24, 27] Overall, the radiuses of stereo-mixed micelles were shown to increase with time, particularly at higher temperatures, which indicate an increase of aggregation number in each micelle. The **L-long/D-long** micelles (Figure 7a), however, displayed minimum change

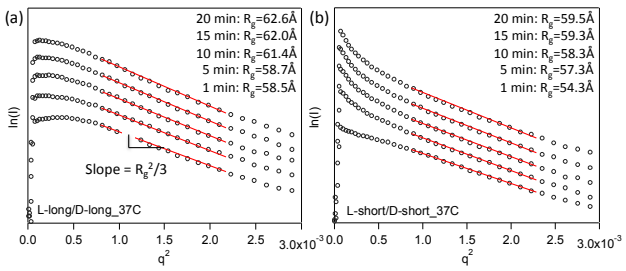

Figure 6. Typical Guinier plots for SANS data taken from a) **L-long/D-long** and b) **L-short/D-short** micelle mixtures at 37°C (y-axis offset); fitting q-range: 0.026-0.046Å.

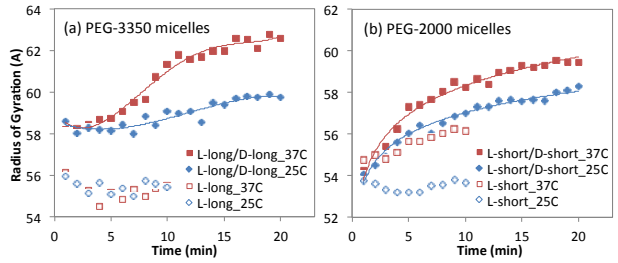

Figure 7. Time-resolved plots for radius of gyration (R_g) form SANS Guinier plot fitting; a) long-PEG and b) short-PEG micelle series.

(below 2 Å increase) at 25°C. At 37°C, the **L-long/D-long** system showed a delay in radius increase in contrast to the immediate increase for the **L-short/D-short** micelle system (Figure 7b). This result is consistent with the slow chain exchange behavior in our hypothesis.

Model dependent kinetic analysis: long PEG micelles

The PLA-PEG-PLA triblock copolymers reported in this study are expected to form flower-type spherical micelles. The scattering data were analyzed using the core-shell model for spherical particles having a polydisperse core with a constant shell thickness. The model accounts for a spherical core composed of the hydrophobic PLA blocks surrounded by a shell of PEG having a constant shell thickness. Tew et al. reported detailed SANS study on the nanostructure of PLA-PEG-PLA triblock copolymer micelles in solution and gel state.[10] Some of the fitting parameters and assumptions have been adopted in this study. The total small angle scattering intensity I(Q) of a core-shell particle in solution can be expressed by Eq 2. Where $\Delta\rho$ is the contrast between the micelle and the solvent, ρ is the term for scattering length density (SLD), N is the volume fraction of solute particles (particle number density), P(Q) is the ***particle form factor***, S(Q) is the ***particle structure factor*** and bkg is the incoherent scattering background of the solvent. The form factor P(Q) describes the shape (morphology) and size of the scattering particles and for a spherical core-shell system it is expressed by Eq 3.

$$I(Q) = N(\Delta\rho)^2 P(Q) S(Q) + bkg \quad (2)$$

$$P(Q) = \frac{Scale}{V_s}\left(\frac{3V_c(\rho_c-\rho_s)j_1(qr_c)}{qr_c]} + \frac{3V_s(\rho_s-\rho_{solv})j_1(qr_s)}{qr_s}\right)^2 + bkg \quad (3)$$

where, $j_1(x) = \sin(x) - \cos(x)/x^2$, $r_s = r_c + t$, and $V_i = (4\pi/3)r_i^3$

The SLD of the core (ρ_c), shell (ρ_s) and surrounding medium ($\rho_{solvent}$) are used to determine the contrast between the core and shell and between the shell and surrounding medium. The SLD of the polymer segments were calculated using the molecular structure of the constituents and the density of each block, their numerical values are summarized in Table S2. The density of oligo-PLA was used instead that of bulk crystalline PLA since the degree of polymerization for the PLA block is only ~11 repeating monomer units. Contrast match experiments confirmed the SLD of PLA to be that calculated using oligo-PLA density. The SLD of the core (ρc) and solvent (ρsolvent) were held fixed, while SLD of shell (ρs) was allowed to float during model fitting. The PLA core was assumed to be dry (anhydrous) as others have done previously.[9, 10] The core and shell sizes (micelle dimensions) are determined from the two terms in Eq 3 and the polydispersity in micelle size is calculated by averaging Eq 3 over a Schulz distribution of radii.

The 5 wt% micelle solutions used in this SANS study are considered non-dilute solutions; therefore, the interference between particles is no longer negligible and the inter-particle structure factor S(Q) contributes to the overall scattering intensity. The time-resolved scattering profiles of the **L-long** and **L-long/D-long** micellar solutions show the possible emergence of a correlation peak at q value between 0.02-0.03 $Å^{-1}$. We considered attractive rather than repulsive micelle-micelle interactions and the Baxter model for hard spheres with short-range attractive interactions was used to describe the time resolve data. We found fine fits to the time resolved data using the core-shell sticky hard sphere (core-shell_SHS) model, and temperature effects on scattering intensity did not produce non-physical solutions to the model fit (Figure S3 and S4). The "goodness-of-fit" or statistical chi-squared information is presented as reduced chi-squared sqrt(X^2/N) (Table S4), where N is the number of data points. A value of one would indicate the model fit to the scattering data is within one standard deviation of each data point, thus being truly best representative of the data.[22] The reported reduced chi-squared values for the long-PEG series are close to one, indicating good statistical fit.

The core-shell_SHS model assumes the micelles are not smooth surfaced hard spheres but have an adhesive "sticky" surface of interpenetrating polymer chains between neighboring micelle. The model has been applied previously to describe the intermicellar correlation of PEO-PPO-PEO[28, 29] and PPO-PEO-PPO[30] spherical micelles. The hard sphere intermicellar interactions and adhesion of the PEG rich surface are shown to depend on temperature and concentration. Baxter introduced a "stickiness parameter" τ defined as τ = 1/12ϵ exp(U_0/kT) to express the attractive potential of the square well. The value of tau is directly related to the strength of the interaction with higher values indicating stronger attraction. The sticky hard sphere (SHS) structure factor is expressed by Eq 4, detailed analytical expression can be found elsewhere.[29, 31]

$$\frac{1}{S(Q)} - 1 = 24\Phi\left[\alpha f_2(Q) + \beta f_3(Q) + \frac{1}{2}\alpha\Phi f_5(Q)\right] + \Phi^2\lambda^2 f_1(Q) - 2\Phi\lambda f_0(Q) \quad (4)$$

Figure 8 plotted the time-resolved data of core radius (a), shell thickness (b), and stickiness (c) for long PEG micelle series (Table S4). Both core radius and shell thickness were found to increase with time for stereo-mixed **L-long/D-long** samples. The micelle diameter was calculated from those values, thus, showed slight or moderate increase in size. As the original 5 wt% **L-long** micelles were characterized to be ca. 20 nm in hydrodynamic diameter by DLS (Table S3), this SANS fitting data showed good agreement for spherical micelles. The micelle radius (core radius + shell thickness) obtained by this model fitting was also consistent with the radius of gyration analyzed by Guinier plot in Figure 6. The scattering intensity I(Q) is related to the scattering contrast of each particle ($\Delta\rho$), particle form factor (P(Q)), and particle structure factor (S(Q)) as explained in Eq 2 above. The 5 wt% micelle solution is considered to be a non-dilute solution. Some degree of increase of the scattering intensity at higher temperature shown in SANS curves can be explained by: 1) the contrast change by dehydration ($\Delta\rho$), 2) the inter-micelle interaction (structure factor), and 3) morphological reorganization or size change (form factor). Each discussion is as follows. 1) The scattering length density of PEG shell layer showed negligible changes within 10 or 20 minutes for all samples. Therefore, contribution of the contrast changes between D_2O and shell, and shell and core to the scattering intensity would be quite small compared to the particle size contribution. 2) The inter-micelle interaction can be estimated by the parameter, stickiness (tau). Figure 8c plots time-resolved stickiness values of **L-long** micelle and **L-long/D-long** micelle solutions at different temperature. The graph shows immediate inter-micelle interaction by the sudden drop of tau values, and subsequent slow decrease. The smaller Tau values at higher temperatures are reasonable as the inter-micelle interaction is expected to be large. Note that the micelle interaction for the single micelle (**L-long**) and stereo-mixture (**L-long/D-long**) are identical, which is theoretically reasonable. Consequently, the structure factor does not explain the unique increase of scattering intensity only for stereo-mixed micelle solution. 3) Core radius and shell thickness in Figure 8a, 8b showed unique increases for only stereo-mixed micelle system. Similar to the data in Guinier analysis (Figure 7a), delayed, but significant size increase for both shell and core are seen at higher temperature. The increase in SANS scattering intensity for **L-long/D-long** system in SANS curves shown earlier is considered due to the increase of aggregation numbers in micelles and probably the structural reorganization driven by stereocomplexation of PLLA and PDLA blocks. The model fitting data explain this discussion; the particle form factor, P(Q), of the single isomeric micelles is very small or negligible, whereas P(Q) of stereo-mixed micelles is significant.

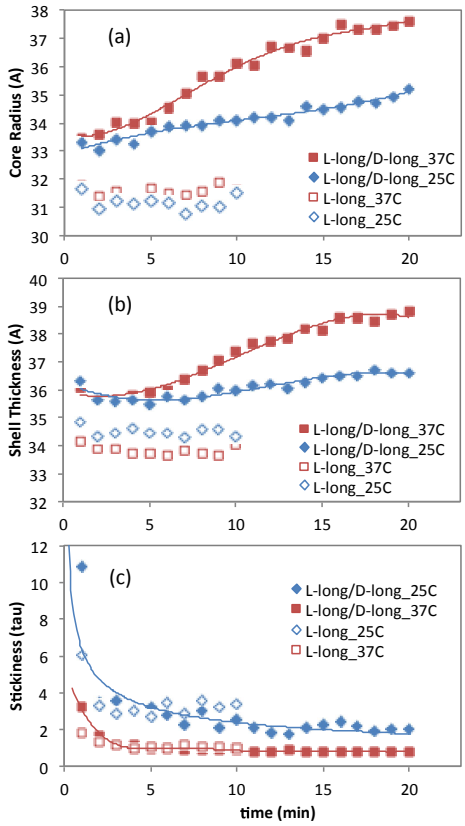

Figure 8. Time-resolved plots for long-PEG series form SANS core-shell SHS model fitting data; a) core radius, b) corona thickness, and c) stickiness

These results support our hypothesis illustrated in Figure 1, which is, the single micelles and stereo-mixed micelles are equilibrium and non-equilibrium chain exchange systems, respectively.

Model dependent kinetic analysis: short PEG micelle

The SANS data of PEG 2000 series were also analyzed using Core-Shell SHS model fitting. Using reasonable fixed parameters, we obtained decent fitting results for all SANS data (Figure S5 and S6). Figure 9 plotted the time-resolved data of core radius (a), shell thickness (b), and stickiness (c) for short PEG micelle series (Table S5).Large increase in core radius can be seen for stereo-mixed micelles even at 25°C (Figure 9a), but the change in shell thickness was not conclusive (Figure 9b). The core and shell size ranges, temperature dependence, and uniqueness of stereo-mixed micelles were all in agreement with other analyses thus far, and similar discussion with long-PEG series can be applied to these short-PEG systems. The form factor (P(Q)) and structure factor (S(Q)) contribute to the increase of SANS intensity particularly at high temperature, while uniqueness of **L-short/D-short** system would be from the increase of aggregation number in each micelle due to the irreversible chain exchange mechanism. Upon further examination, it is

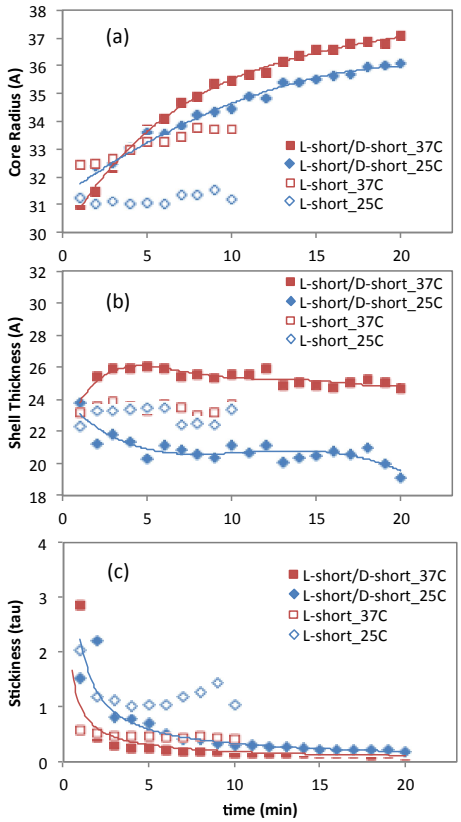

Figure 9. Time-resolved plots for short-PEG series form SANS core-shell SHS model fitting data; a) core radius, b) shell thickness, and c) stickiness

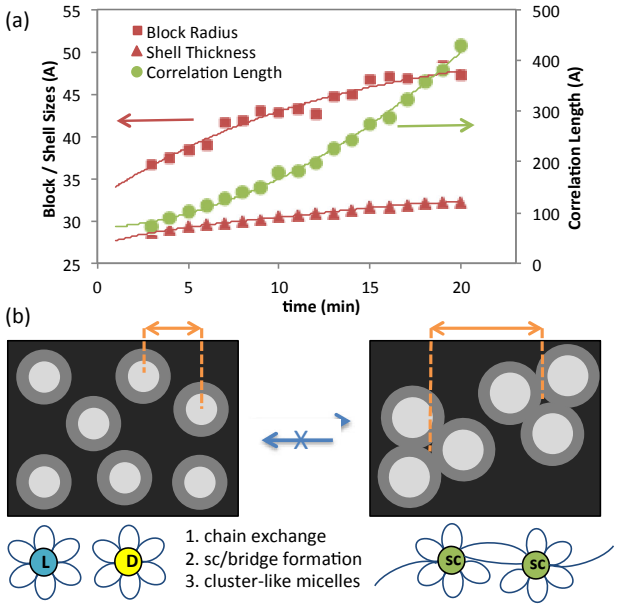

Figure 10. (a) Time-resolved plots for short-PEG series at 37°C by SANS Fractal PolyCore model fitting; block radius (square), shell thickness (triangle), and correlation length (circle). (b) Conceptual illustration of the chain exchange, stereocomplex formation, and structural reorganization of the mixture of PLLA-PEG-PLLA/PDLA-PEG-PDLA micelles (non-equilibrium micelle system).

evident that the short-PEG data fit to the core-shell SHS model begins to deviates at higher temperature and time interval, as can be seen by the increase in the reduced chi-squared values (Table S5). As previously discussed, SANS curves for the stereo-mixture of short PEG micelles display significant changes for both intensity increase and low-q shift within 20 minutes (Figure 5). The time resolved scattering profiles for the **L-short** and **L-short/D-short** samples exhibited characteristic features for scattering from clusters or aggregate (i.e., lack of an intermicellar correlation peak and increase in intensity at low-q), rather than from individual micelles interacting though a hard sphere potential. We considered that the fractal model would yield a better fitting for this irreversible rapid chain-exchange micelle system. We modelled the scattering data for the **L-short** and **L-short/D-short** polymer solutions using Teixeira's model for scattering from fractal-like cluster/aggregates.[32, 33] The structure factor is expressed by Eq 5.

$$S(Q) = 1 + \frac{\sin[(D_f-1)\tan^{-1}(q\xi)]}{(qR_o)^{D_f}} \frac{D_f\Gamma(D_f-1)}{[1+1/(q^2\xi^2)]^{(D_f-1)/2}} \qquad (5)$$

where $\Gamma(x)$ is the gamma function, ξ is the large size cut off in the aggregates density distribution function and D_f is the fractal dimension. The fractal dimension, D_f, is a term utilized to describe the self-similarity of the mass fractal structure. The value of D_f can vary from 1 for loosely arranged clusters to 3 for compact clusters. For our model fitting, we obtained the best fit for D_f = 1.55, indicating a loosely connected aggregates with imprecise interfaces. This is a reasonable assumption since at the SANS measurement temperatures of 25°C and 37°C the micellar solution is at an early stage of network formation. The cut-off distance ξ can be used to describe the size of the aggregate or the correlation length between scattering mass centers as others have done previously. [34] We obtained fine fits of the scattering data to the Fractal PolyCore model, particularly for high temperature and time intervals (Figure S7, Table S6). The model considers scattering from a fractal structure with a primary building block of polydisperse core-shell spheres. Figure 10a plots changes in sizes (left axis) and correlation length (right axis) for short PEG stereo-mixed micelle solution at 37°C. Here, increase of block radius is visible in 20 minutes. As seen in SANS profile in Figure 5b, **L-short/D-short** system doesn't show the peak in the range of 0.01-0.1 q $Å^{-1}$. Because of the rapid chain exchange between L- and D-micelles, it is presumed that the PEG bridges form locally and the original micelles become clusters in early stage. Although hydrogel formation is recognized around 60°C for 5 wt% **L-short/D-short** system, SANS data clearly indicates the chain exchange and cluster forming as a seed of the network gel rapidly at 37°C and in slower rate at room temperature. With fully hydrated and homogeneous original micelle form, inter-micelle distance is supposed to be small enough. As micelles associate by chain exchange to grow into clusters,

inter-cluster distance must increase with time as explained above in the fitting theory. The correlation length is related to either the cluster size or distance between centers of the clusters, of which we observe rather exponential growth in Figure 10a. This **L-short/D-short** micelle mixture exhibits a rapid chain exchange and stereocomplex formation in each micelle core. Extended PEG bridges form the clusters as illustrated in Figure 10b. Those clusters then continue to grow towards fully networked hydrogel form. As increasing the degree of extended PEG bridge formation, micelle shell thickness would also increase as the model fitting data shows.

Conclusion

The dynamic chain exchange behaviour of the micelles consisting of enantiomeric triblock copolymers, PLLA-PEG-PLLA and PDLA-PEG-PDLA, in aqueous medium was analyzed using TR-SANS technique. The scattering data of the single and stereo-mixed micelles showed dependence on the PEG block length, temperature and time. Considerable differences in time dependence of the scattering intensity were observed between single L-micelles (small or negligible) and L/D stereo-mixed micelles (significant) as a factor of temperature. Furthermore, the SANS data of the micelles with PEG molecular weight 2000 and 3350 (Da) displayed distinct difference in the scattering profiles. Model dependent analysis of the scattering data allows interpretation of the kinetics occurring with the chain exchange. The model fitting data showed time dependent increase of micellar dimension (core radius + shell thickness) for the stereo-mixed micelles only, which occurs due to the increase of aggregation numbers in micelles, and structural reorganization driven by stereocomplexation of PLLA and PDLA blocks. These results support our hypothesis illustrated in Figure 1, which is, chain exchange of the single micelles and stereo-mixed micelles are equilibrium and non-equilibrium, respectively. The TR-SANS data also revealed that the size of the shell forming block of the flower-type micelles influences the chain exchange kinetics. Guinier plot analysis and model fitting data concurrently indicate a delay in increase of micelle dimension (aggregation number) for long-PEG series, while an immediate increase was observed for short-PEG series. Moreover, the PEG 3350 series indicated scattering arising from individual micelles interacting though an attractive hard sphere potential; while the scattering from the PEG 2000 series was indicative of scattering from fractal-like cluster/aggregates. Given that increase in micelle dimension is the result of stereocomplexation between PLLA/PDLA micelles, these results support our experimental observation shown in Figure 3, which is, the short-PEG series undergoes faster chain exchange between micelles compared to the long-PEG series.

Acknowledgements

We acknowledge the support of the National Institute of Standards and Technology, U.S. Department of Commerce, in providing the neutron facilities used in this work. Special thank is to Dr. Paul Butler at CNMS, NIST for his helpful advices and discussion on SANS experiments.

References

1 G. S. Kwon and K. Kataoka, Advanced Drug Delivery Reviews, 1995, 16, 295-309.
2 P. Hu and N. Tirelli, Reactive & Functional Polymers, 2011, 71, 303-314.
3 A. Tripathi, K. C. Tam and G. H. McKinley, Macromolecules, 2006, 39, 1981-1999.
4 M. T. Proetto, A. M. Rush, M. P. Chien, P. A. Baeza, J. P. Patterson, M. P. Thompson, N. H. Olson, C. E. Moore, A. L. Rheingold, C. Andolina, J. Millstone, S. B. Howell, N. D. Browning, J. E. Evans and N. C. Gianneschi, Journal of the American Chemical Society, 2014, 136, 1162-1165.
5 C. Chaibundit, G. Ricardo, V. Costa, S. G. Yeates and C. Booth, Langmuir, 2007, 23, 9229-9236.
6 R. Lund, L. Willner, V. Pipich, I. Grillo, P. Lindner, J. Colmenero and D. Richter, Macromolecules, 2011, 44, 6145-6154.
7 R. Lund, L. Willner, D. Richter and E. E. Dormidontova, Macromolecules, 2006, 39, 4566-4575.
8 R. Lund, L. Willner, D. Richter, H. Iatrou, N. Hadjichristidis and P. Lindner, Journal of Applied Crystallography, 2007, 40, S327-S331.
9 T. Riley, C. R. Heald, S. Stolnik, M. C. Garnett, L. Illum, S. S. Davis, S. M. King, R. K. Heenan, S. C. Purkiss, R. J. Barlow, P. R. Gellert and C. Washington, Langmuir, 2003, 19, 8428-8435.
10 S. K. Agrawal, N. Sanabria-DeLong, G. N. Tew and S. R. Bhatia, Macromolecules, 2008, 41, 1774-1784.
11 C. C. Lin and A. T. Metters, Advanced Drug Delivery Reviews, 2006, 58, 1379-1408.
12 S. R. Van Tomme, G. Storm and W. E. Hennink, International Journal of Pharmaceutics, 2008, 355, 1-18.
13 C. L. He, S. W. Kim and D. S. Lee, Journal of Controlled Release, 2008, 127, 189-207.
14 B. Jeong, Y. H. Bae, D. S. Lee and S. W. Kim, Nature, 1997, 388, 860-862.
15 B. Jeong, S. W. Kim and Y. H. Bae, Advanced Drug Delivery Reviews, 2002, 54, 37-51.
16 K. A. Aamer, H. Sardinha, S. R. Bhatia and G. N. Tew, Biomaterials, 2004, 25, 1087-1093.
17 T. Fujiwara, T. Mukose, T. Yamaoka, H. Yamane, S. Sakurai and Y. Kimura, Macromolecular Bioscience, 2001, 1, 204-208.
18 T. Mukose, T. Fujiwara, J. Nakano, I. Taniguchi, M. Miyamoto, Y. Kimura, I. Teraoka and C. W. Lee, Macromolecular Bioscience, 2004, 4, 361-367.
19 D. G. Abebe and T. Fujiwara, Biomacromolecules, 2012, 13, 1828-1836.
20 Z. Li, D. Yuan, X. Fan, B. H. Tan and C. He, Langmuir, 2015, 31, 2321-2333.
21 R. P. May, K. Ibel and J. Haas, Journal of Applied Crystallography, 1982, 15, 15-19.
22 S. R. Kline, Journal of Applied Crystallography, 2006, 39, 895-900.
23 H. Tsuji, F. Horii, M. Nakagawa, Y. Ikada, H. Odani and R. Kitamaru, Macromolecules, 1992, 25, 4114-4118.

24 H. Hussain, B. H. Tan, G. L. Seah, Y. Liu, C. B. He and T. P. Davis, Langmuir, 2010, 26, 11763-11773.
25 I. Goldmints, G. E. Yu, C. Booth, K. A. Smith and T. A. Hatton, Langmuir, 1999, 15, 1651-1656.
26 L. Yang, P. Alexandridis, D. C. Steytler, M. J. Kositza and J. F. Holzwarth, Langmuir, 2000, 16, 8555-8561.
27 Y. Tu, X. Wan, D. Zhang, Q. Zhou and C. Wu, Journal of the American Chemical Society, 2000, 122, 10201-10205.
28 Y. C. Liu, S. H. Chen and J. S. Huang, Physical Review E, 1996, 54, 1698-1708.
29 Y. C. Liu, S. H. Chen and J. S. Huang, Macromolecules, 1998, 31, 2236-2244.
30 K. Mortensen, W. Brown and E. Jorgensen, Macromolecules, 1994, 27, 5654-5666.
31 C. Regnaut and J. C. Ravey, Journal of Chemical Physics, 1989, 91, 1211-1221.
32 J. Teixeira, Journal of Applied Crystallography, 1988, 21, 781-785.
33 Z. L. Quan, K. Z. Zhu, K. D. Knudsen, B. Nystrom and R. Lund, Soft Matter, 2013, 9, 10768-10778.
34 F. A. Campo and E. J. Barbero, Journal of Non-Crystalline Solids, 2012, 358, 721-727.

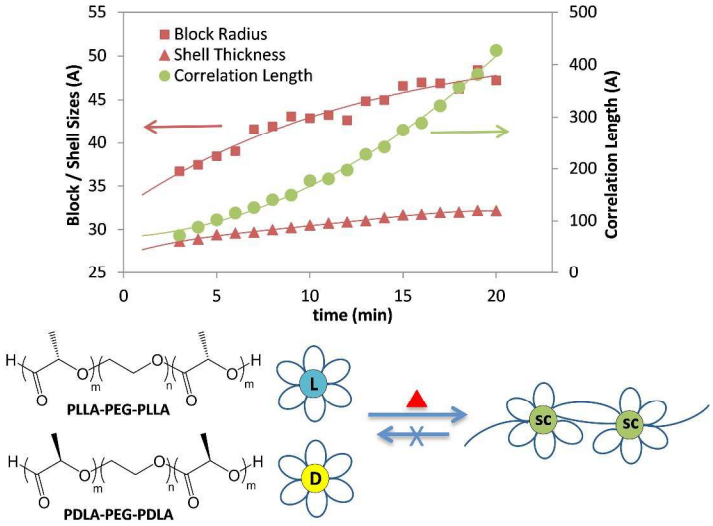

TR-SANS study has revealed the initial stage of non-equilibrium micelle chain exchange for the thermo-responsive hydrogel system by stereocomplexation.